On the Sound Generation and its Controls in Turbulent Combustion Field

Mamoru TANAHASHI, Shunsuke TSUKINARI, Toshihiko SAITOH, Toshio MIYAUCHI
Department of Mechanical and Aerospace Engineering, Tokyo Institute of Technology,
2-12-1 Ookayama, Meguro-ku, Tokyo 152-8552, Japan

Gyung-Min CHOI
National Aerospace Laboratory,
7-44-1 Jindaiji-Higashi, Chofu, Tokyo 182-8522, Japan

Masaru IKAME, Takeyuki KISHI, Kazuyoshi HARUMI, Katsuhide HIRAOKA
National Maritime Research Institute,
6-38-1, Shinkawa, Mitaka-shi, Tokyo, 181-0004, Japan

In this study, DNS of compressible, chemically reacting turbulent mixing layer has been performed to clarify the mechanism of sound generation in turbulent combustion field. The effects of heat release on the mechanism of sound generation are investigated in fully developed turbulent state. The contributions of sound source terms are investigated from DNS results. The acoustic source is dominated by the entropy term. The distributions of the Reynolds stress term and the entropy term are investigated by focusing on the heat release rate and the coherent fine scale eddy in turbulence. The Reynolds stress term shows similar structure with the coherent fine scale eddies. The distribution of the entropy term is mainly dominated by the heat release rate, while it is affected by the energy dissipation rate around the coherent fine scale eddy in the region with low heat release rate. The far field pressure fluctuation was also predicted using acoustic analogies. By comparing the predicted far field sound with DNS result, Lighthill's and Powell's acoustic analogies are evaluated. For turbulent flames, the far field sound seems to be predicted only by considering the entropy term, while the Reynolds term should be included to predict the sound radiated in the process of the transition to turbulence. Based on the investigation on the sound generation mechanism in turbulent flames, a passive control is applied to a coaxial dump combustor and noise reductions are demonstrated as a preliminary step for developing the active control scheme of the combustor. Finally, effectiveness of CH PLIF measurement as for an indicator of the heat release rate is shown by comparing results of CH PLIF experiments and numerical simulations including DNS with a detailed kinetic mechanism.

1. Introduction

In the development of high efficiency combustor, it is important to reduce the combustion noise and to inhibit the combustion-driven oscillations. Combustion noise is produced by unsteady oscillations of the flame, which is due to the interaction between the vortex structures and flame in the shear flows. Combustion-driven oscillations are caused by resonant interaction between the combustion noise and a natural frequency of the combustor. In order to understand and control these phenomena, it is necessary to clarify the mechanism of sound generation in chemically reacting turbulent flows.

With the recent development of the computer technology, researches on the sound generation in the non-reacting flows become possible by direct numerical simulation (DNS) (Colonius *et al.* 1994, Lilley *et al.* 1994, Mitchell *et al.* 1995, Colonius *et al.* 1997). From the exact numerical results both in the near field and the far field, details of the acoustic source have been investigated and acoustic analogies such as Lighthill (1952) and Powell (1964) have been validated. However, almost all previous studies were restricted to two-dimensional and non-reacting cases due to the limitation of the computer resources. Therefore, the knowledge of the sound source and the acoustic analogies can not be applied directly to predictions of the sound in the turbulent combustion field.

Recently, active feedback controls of the combustor have been reported by many researchers (Paschereit *et al.* 1999, Lee *et al.* 2000, Harper *et al.* 2001). The active controls have possibilities to develop quite high efficiency and stable combustors. However, the active controls may take high costs for developing control devices and constructing combustor. Therefore, it is required to control the combustor passively before applying the active controls as possible. The factors which are difficult to be controlled passively should be controlled actively. To develop active control scheme of the combustors, the understandings of the flame structures in combustor is quite important. Due to remarkable developments of the laser diagnostics of the combustion field, detailed structure of the turbulent flames can be measured by a particle image velocimetry (PIV), a planar laser-induced fluorescence (PLIF) etc. Especially, CH PLIF measurements have been used to investigate the flame fronts in turbulence because CH radicals are produced at the flame front and have very narrow width enough to represent the reaction zone (Allen *et al.* 1986, Monsour *et al.* 1998, Carter *et al.* 1998). Furthermore, it is well known that distribution of CH radicals agrees with that of the heat release rate. Since the heat release rate plays important roles in the sound generation mechanism in turbulence combustion field, CH PLIF measurement may provide the information about spatial and temporal fluctuations of the heat release rate. By understandings spatial and temporal fluctuations of the heat release rate in the combustor, the development of the active controls scheme becomes easier because the dominant sound source can be identified in the developing process.

In this study, DNS are extended for investigations of the sound generation in the turbulent combustion in section 2. DNS of a compressible and chemically reacting turbulent mixing layer is conducted and the mechanism of the sound generation in the turbulent flames is clarified. The accuracy of the acoustic analogies is also evaluated by comparing DNS results and solutions of the wave equations in the far field. In section 3, a passive control is applied to a coaxial dump combustor based on the results in section 2 and noise reductions are demonstrated as a preliminary step for developing the active control scheme. In section 4, effectiveness of CH PLIF measurement as for a indicator of the heat release rate is shown by comparing results of CH PLIF experiments and numerical simulations including DNS with a detailed kinetic mechanism.

2. Sound Generation Mechanism in Turbulent Combustion Field

2.1 Direct numerical simulation of reacting mixing layer

In this study, we assumed that the external forces, Soret effect, Dufour effect, pressure gradient diffusion, bulk viscosity and radiative heat transfer could be negligible. The chemical reaction is idealized to be a single step, irreversible reaction: A+B $\Rightarrow$ 2P+ΔH, where ΔH is the heat release with the chemical reaction. The reaction rate, thermal properties and transport properties are assumed to be independent on the temperature. These assumptions are enough to discuss the sound generation mechanism in the turbulent flames. DNSs of a temporally-developing, compressible turbulent mixing layer with and without chemical reaction are conducted to investigate the effects of heat release on the sound generation in turbulence. Periodic boundary conditions are applied in the streamwise (x) and spanwise (z) directions, and NSCBC (Poinsot & Lele 1992, Baum *et al.* 1994) are used in the transverse (y) direction. The governing equations are discretized by the spectral method in the x and z direction, and by the fourth-order central finite difference scheme in the y direction. A third-order low storage Runge-Kutta scheme is used for time integration. The computational domain in the x, y and z direction is selected to be 2Λ, 6Λ and $4\Lambda/3$ respectively, where Λ is the most unstable wavelength for the initial mean velocity profile.

The initial velocity field is composed of a hyperbolic tangent streamwise velocity and three-dimensional random perturbations which include the banded white noise (Tanahashi *et al.* 2001). The initial mass fraction of chemical species are given by Y_A=0.5+0.5tanh(2y-y_0), Y_B=0.5-0.5tanh(2y-y_0) and Y_P=1.0- Y_A-Y_B, where y_0 represents the initial overlap parameter of the reactants, and is selected to be y_0=1.0 in the present study. The DNSs are performed on the mesh of $120\times1921\times80$ and are conducted for Re=600, Pr=0.7, Sc=0.7 and γ=1.4. All variables are non-dimensinalized by density and temperature in free streams, the initial vorticity thickness and velocity difference across the shear layer. The convective Mach number (Papamoschou & Roshko 1988) is selected for Mc=0.2. To investigate heat release effect on the sound generation, DNS are conducted for two cases: one is the reacting case with Da=2.0 and Ce=1.0, the other is the non-reacting case with Da=0.0 and Ce=0.0, where Da and Ce represent Damkohler number and non-dimensional heat release (McMurtuy *et al.* 1989).

2.2 Turbulence structure and heat release rate

Figure 1 shows contour plots of the second invariant of the velocity gradient tensor and heat release rate at t=80. The second invariant is defined by $Q=(W_{ij}W_{ij}-S_{ij}S_{ij})/2$, where S_{ij} and W_{ij} denote symmetric and asymmetric parts of the velocity gradient tensor, respectively. At t=80, energy spectrum in the streamwise direction shows -5/3 power law, and the flow field attains fully-developed turbulent state. Our recent studies on the fine scale structure of turbulence (Tanahashi *et al.* 1997a, 1997b, 2001,) have shown that turbulence is composed of a universal fine scale structure: coherent tubelike eddies, and these coherent fine scale eddies of turbulence are well represented by the positive Q region in turbulence.

With the transition to turbulence, lots of fine scale eddies appear in the shear layer as shown in Fig. 1, which indicates that the turbulence transition can occur even though the heat is released by the chemical reaction, and temperature becomes high and density decreases in the center of the shear layer. McMurtry *et al.* (1989) have shown that the heat release rate in the reacting mixing layers shows large values between the Kelvin-Helmholtz rollers (the braid region) before the transition. Figure 1 implies that the heat release rate is still concentrated in the braid region even after the transition. However, in the core region, small

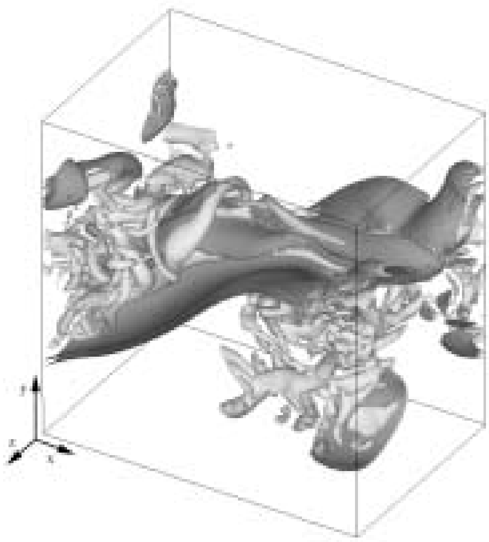

Fig. 1 Distributions of the second invariant (Q) and heat release rate ($DaCe\rho^2Y_AY_B$) at t=80. Gray: Q=0.15 and dark gray: $DaCe\rho^2Y_AY_B$=0.02.

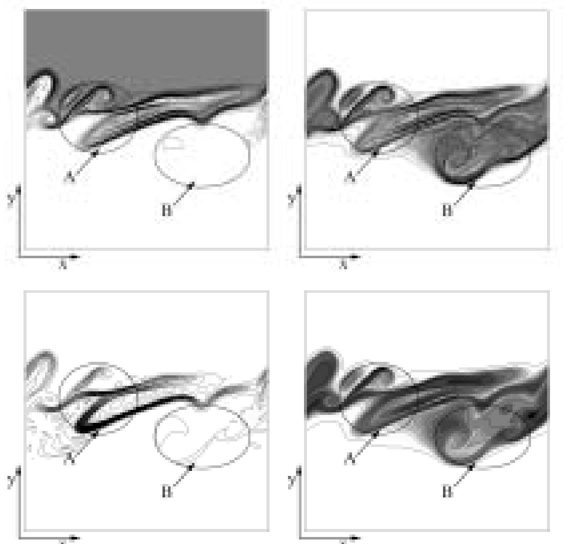

Fig. 2 Distributions of mass fraction of reactant A (a), mass fraction of product (b), heat release rate (c) and temperature (d) in a typical x-y plane (z=2/3Λ) at t=80.

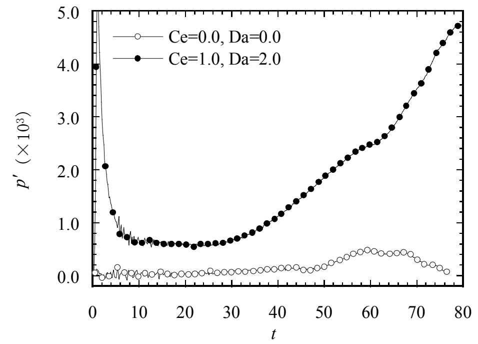

Fig. 3 Temporal evolution of pressure fluctuations in the far field.

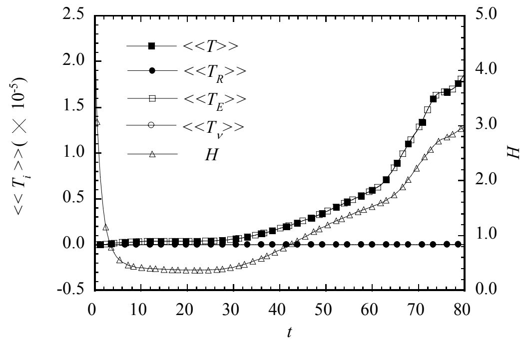

Fig. 4 Evolutions of acoustic source terms in Lighthill's acoustic analogy and the total heat release rate.

wrinkles of the heat release rate can be observed due to the interaction between the coherent fine scale eddy and the chemical reaction. Similar to the case of the turbulent premixed flames (Tanahashi *et al.* 2000), these coherent fine scale eddies play important roles on the local structure of the turbulent non-premixed flames because their strong swirling motion enhances mixing and reaction in turbulence.

Figure 2 shows the distributions of reactant A, product, heat release rate and temperature in a typical x-y plane at t=80. With the turbulence transition, the distributions of these properties become complicated significantly. Two typical structures can be observed in the fully-developed turbulent reacting mixing layer. In region A, which is denoted by a circle A in Fig. 2, reactant and product concentrations and temperature are relatively high, and high heat release rate region can be observed. The region A corresponds to the braid region in Fig. 1. On the other hand, in region B denoted by a circle B, the reactant concentration is low, whereas the product concentration and temperature is very high. In this region, heat release rate shows quite low value because the reactants are completely consumed.

2.3 Effects of heat release on the sound generation

Figure 3 shows the temporal evolution of pressure fluctuation in the far field. The measurement point is located at y=3Λ. The time coordinate is modified by considering the sound propagation from the center of the shear layer to the measurement point. Therefore, the evolution of pressure fluctuation in Fig. 3 can be compared directly to turbulence and flame dynamics in the near field. The pressure fluctuation obtained for the non-reacting case is also plotted for comparison. The abrupt increase of pressure fluctuation in the initial period (t < 4) is due to the initial conditions of the reactants. Figure 3 suggests that the amplitude of pressure fluctuation generated in reacting turbulent mixing layer is larger than that in the non-reacting mixing layer. In the non-reacting case, the pressure fluctuation decreases significantly

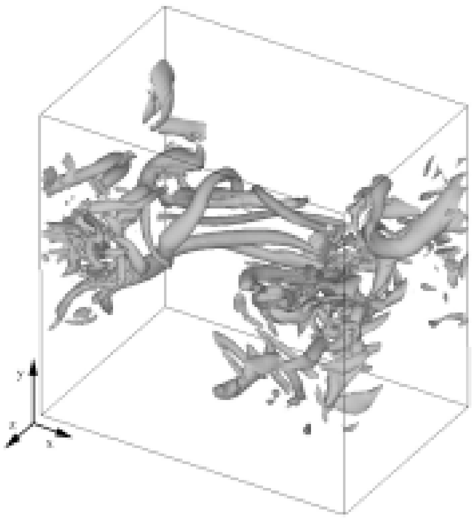

Fig. 5 Contour surfaces of Reynolds stress term of the acoustic source (T_R=-0.4)

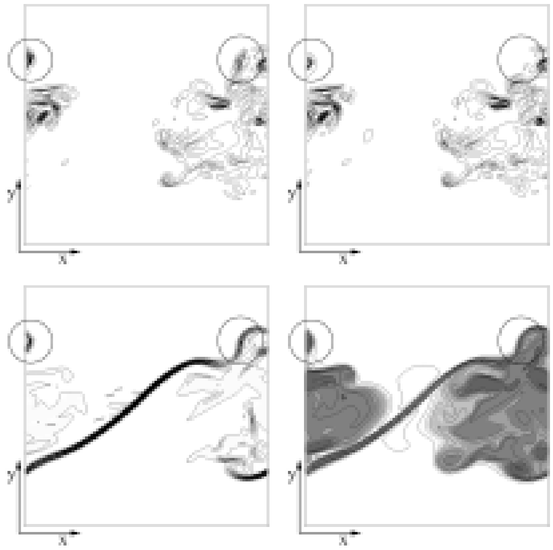

Fig. 6 Distributions of Reynolds stress term (a), the second invariant (b), heat release rate (c) and density (d) in a typical *x*-*y* plane (*z*=0) at *t*=80.

after the transition to turbulence ($t > 65$). However, the pressure fluctuation increases continuously even after the transition for the reacting case. Furthermore, the growth rate of pressure fluctuation after mixing transition ($t > 65$) is higher than that in the period of the transition ($35 < t <6$ 0) for the reacting case. The reason of these differences is that the sound generation is determined by the vortex motion in the non-reacting turbulence, while that is dominated by the heat release rate in the reacting turbulence.

As an acoustic analogy, Lighthill (1952) has rearranged the exact continuity and momentum equations into a wave equation as follow:

$$\frac{\partial^2 \rho'}{\partial t^2} - \frac{1}{M^2}\frac{\partial^2 \rho'}{\partial x_i \partial x_i} = \frac{\partial^2 T_{ij}}{\partial x_i \partial x_j}, \tag{1}$$

where T_{ij} is the Lighthill's turbulent stress tensor defined by

$$T_{ij} = \rho u_i u_j + \frac{1}{M^2}\delta_{ij}\left(\frac{1}{\gamma}p - \rho\right) - \frac{1}{\mathrm{Re}}\tau_{ij}. \tag{2}$$

In this study, the total acoustic source term (T) is decomposed into Reynolds stress term (T_R), entropy term (T_E), and viscous term (T_V) as follows:

$$T_R = \frac{\partial^2(\rho u_i u_j)}{\partial x_i \partial x_j},\quad T_E = \frac{\partial^2}{\partial x_i \partial x_j}\left[\frac{1}{M^2}\delta_{ij}\left(\frac{1}{\gamma}p - \rho\right)\right],\quad T_V = \frac{\partial^2}{\partial x_i \partial x_j}\left(-\frac{1}{\mathrm{Re}}\tau_{ij}\right), \tag{3}$$

$$T = T_R + T_E + T_V. \tag{4}$$

Furthermore, a following integral of acoustic source terms are introduced to evaluate the magnitude of each acoustic source term:

$$<< T_k >>= \iiint T_k^2\, dxdydz, \tag{5}$$

Figure 4 shows the contributions of acoustic source term in Lighthill's acoustic analogy in the reacting case. In the non-reacting turbulent mixing layer, the order of Reynolds stress term and entropy term is nearly the same because the entropy term has effective values due to the turbulent energy dissipation in the three-dimensional turbulence. It should be noted that the entropy term in the two-dimensional non-reacting case is negligibly small (Li *et al.* 2001). In the reacting case, however, the entropy term becomes significantly larger than the Reynolds stress term and the viscous term. Figure 4 includes the temporal evolution of total heat release rate defined by

$$Q = CeDa\iiint \rho^2 Y_A Y_B\, dxdydz. \tag{6}$$

The evolution of the entropy term is similar with that of the total heat release rate. Moreover, the evolutions of the total heat release rate are also consistent with the pressure fluctuation in the far field that is shown in Fig. 3. These results suggest that the sound generation is dominated by the heat release rate in turbulent flames.

In the case of a laminar flame, it has been shown that the fluctuation in heat release rate becomes sound

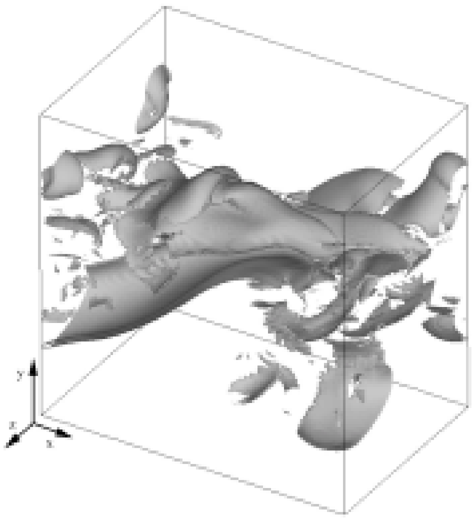

Fig. 7 Contour surfaces of entropy term of the acoustic source (T_E=-20.0)

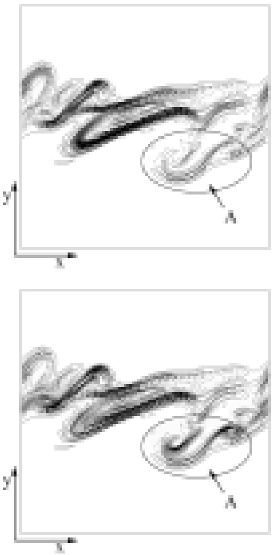

Fig. 8 Contour plots of the entropy term with heat release rate and energy dissipation rate in a typical x-y plane (z=2/3Λ) at t=80. (a): Gray: $DaCe\rho^2 Y_A Y_B$; Lines: T_E, (b): Gray: ε; Lines: T_E.

source in the wave equation (Li *et al.* 2000). In the case of perfect gas, if the variations of all quantities are assumed to be small, the continuity and energy conservation equations can be linearised to the following two equations (Lighthill 1978, Tanahashi *et al.* 1995).

$$\frac{\partial \rho'}{\partial t} = -\rho_0 d\ , \tag{7}$$

$$\frac{\partial p'}{\partial t} = -\gamma p_0 d + q\ , \tag{8}$$

where q represents the total heat release rate. From the above linearised energy equation (Eq. (8)), the variation of pressure fluctuation can be related to the total heat release rate. By using these two equations and the definition of entropy component, the entropy component can be expressed by the following equation.

$$T_E = \frac{\partial^2}{\partial x_i x_j}\left[(p - p_0) - c^2(\rho - \rho_0)\right] = \frac{\partial^2}{\partial x_i x_j}\left(\frac{q}{\rho_0 d}\right). \tag{9}$$

The above equation shows that the entropy component is determined by the second spatial derivative of the total heat release rate. In the case of the turbulent flames, the heat release rate shows large fluctuations as shown in the above, and the coherent fine scale eddies also becomes the sound source. Hereafter, detailed structures of the sound source terms are discussed by using DNS data in the fully- developed turbulent state.

Figure 5 shows the contour surfaces of Reynolds stress term of the acoustic source at t=80. With the transition to turbulence, lots of tubelike structures are observed in the core region similar to the second invariant in Fig. 1. This is because that the Reynolds stress term can be exactly expressed by the second invariant as T_R=-2Q in the limit of the incompressible flow. Figure 5 suggests that the relation between these two variables sustained even in the chemically reacting turbulence. Therefore, the coherent fine scale eddy plays important roles in the sound generation not only in non-reacting turbulence but also in reacting turbulence. Figure 6 shows the distributions of the Reynolds stress term, the second invariant, the heat release rate and density in a typical x-y plane at t=80. The increments of the contour plots of the Reynolds stress term and the second invariant are selected to satisfy the relation ΔT_R=2ΔQ, and all the contour lines are plotted by solid lines regardless of positive or negative for convenience. As shown in Fig. 6, overall distribution of the Reynolds stress term is identical to that of the second invariant. However, the differences between Reynolds stress term and the second invariant is observed in the circled regions in Fig. 6. In these regions, large density gradient exists due to high heat release rate. Therefore, relation in the incompressible limit T_R=-2Q is not satisfied in these regions. These results indicate that the heat release affect the Reynolds stress term through the density gradient in reacting turbulent mixing layers.

Figure 7 shows the contour surfaces of the entropy term at t=80. In the non-reacting turbulent mixing

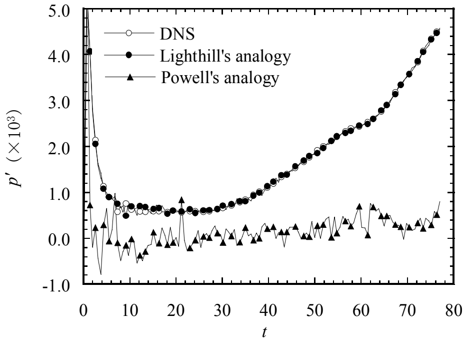

Fig. 9 Comparison of the far field sound obtained by DNS and predicted by Lighthill's and Powell's acoustic analogy.

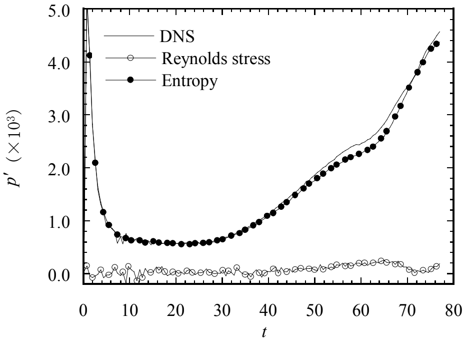

Fig. 10 Contributions of Reynolds stress term and entropy term to the far field sound predicted by Lighthill's acoustic analogy.

layer, the entropy term shows sheet-like structure around coherent fine scale eddies in the fully-developed state. However, in the reacting turbulent mixing layer, the entropy term shows significantly large values in the braid region, not in the core region where coherent fine scale eddies are observed. Compared with the contour surfaces of heat release rate in Fig. 1, it can be seen that the distribution of entropy term is consistent with that of the heat release rate, which are similar to results obtained in the two-dimensional chemically reacting mixing layers (Li *et al.* 2000). To show details of the entropy term, contour plots of the entropy term are superimposed on the distributions of the heat release rate and the turbulent energy dissipation rate on the typical x-y plane in Fig. 8. The turbulent energy dissipation rate (ε) is defined by $\varepsilon = 2\nu S'_{ij}S'_{ij}$, where S'_{ij} represents strain rate tensor of velocity fluctuations from the streamwise average. From these figures, it is clearly shown that the distribution of entropy term is mainly determined by the heat release rate. The entropy term shows negative values in the regions with high heat release rate and shows positive values around these regions. However, in core region denoted by a circle, the entropy term shows relatively large values despite low heat release rate. In these regions, the entropy term coincides with the distribution of the energy dissipation rate. Note that the distribution of entropy term is determined by the energy dissipation rate in the non-reacting turbulence. These results suggest that the entropy term is mainly determined by the heat release rate, while it is influenced by the energy dissipation rate in low heat release rate regions.

2.4 Prediction of far field sound by acoustic analogies

2.4.1 Lighthill's and Powell's acoustic analogies

In the above section, DNS results obtained in the computational domain including near field and acoustic far field were presented. However, this kind of computation is quite difficult in engineering applications because of the following reasons (Crigthon 1975); (i) the acoustic field is significantly large compared with the flow field, (ii) the energy of acoustic field is very small relative to that of the flowfield, (iii) the numerical errors induced by discretization may act as a significant source of sound. Therefore, in general, the computations of full compressible Navier-Stokes equations are carried out only in the near field. The far field sound is predicted by using acoustic analogy with source terms which have been obtained by DNS in the near field. In this section, acoustic analogies are evaluated by comparing the far field sound predicted by acoustic analogies with DNS results.

The Lighthill's equation (Eq. (1)) is an accurate equation rearranged from continuity and Navier-Stokes equations, and clearly shows that the sound is generated in the turbulent flow. However, it is unclear how the sound is generated from the flow field. In order to clarify this problem, Powell (1964) has proposed a theory of vortex sound and deduced the following wave equation.

$$\frac{\partial^2 \rho'}{\partial t^2} - \frac{1}{M^2}\nabla^2 \rho' = \nabla \cdot (\rho \boldsymbol{\omega} \times \boldsymbol{u}). \tag{10}$$

where $\boldsymbol{\omega}$ is vorticity vector. Eq. (10) shows that fluctuation of vorticity plays an important role in the sound generation. Here, it should be noted that the relation between Powell's acoustic source and Lighthill's acoustic source can be expressed by

$$T = \nabla \cdot \left[\rho \boldsymbol{\omega} \times \boldsymbol{u} + \nabla\left(\tfrac{1}{2}\rho \boldsymbol{u}^2\right) - \tfrac{1}{2}\boldsymbol{u}^2 \nabla \rho + \boldsymbol{u}\nabla \cdot (\rho \boldsymbol{u})\right] + T_E + T_V\ . \tag{11}$$

This relation shows that the Powell's acoustic source represents a part of the Lighthill's source.

2.4.2 Far field sound predicted by acoustic analogies

In this study, the far field sound is predicted by the Lighthill's acoustic analogy (Eq. (1)) and the Powell's acoustic analogy (Eq. (10)). In the case of the Lighthill's acoustic analogy, the following wave

Fig. 11 The coaxial dump combustor in National Maritime Research Institute.

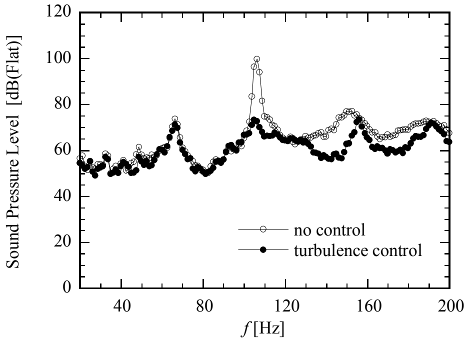

Fig. 12 Spectrums of combustion-induced noise for no control and turbulence control (ϕ=0.4, hydrogen-air flame).

equations are used to evaluate the contribution of each acoustic source term.

$$\frac{\partial^2 \rho'_k}{\partial t^2} - \frac{1}{M^2}\frac{\partial^2 \rho'_k}{\partial x_i \partial x_i} = T_k \,, \tag{12}$$

where T_k is acoustic source term and ρ'_k is density fluctuation in the far field predicted by the acoustic source term T_k. Because the wave equation is a linear equation, the density fluctuation predicted by Lighthill's acoustic analogy can be obtained by summing up all density fluctuations predicted by each acoustic source term: $\rho'_{\mathrm{Lighthill}} = \rho'_{\mathrm{TR}} + \rho'_{\mathrm{TE}} + \rho'_{\mathrm{TV}}$. Numerical methods used in the prediction are the same with DNS except for time advancement and boundary conditions in the y direction. For the time advancement, a second-order Adams-Bashforth scheme is used. Non-reflecting boundary conditions proposed by Engquist *et al.* (1979) are used in the y direction. The computational grids and time step are also same with those used in DNS.

In predicting the far field sound by solving the wave equations, the size of acoustic source used in the prediction is an important parameter (Li *et al.* 2001). In this study, the source size is selected to be 4Λ. In the near field, the wave equations with the acoustic source term obtained by the DNS are solved. On the other hand, the wave equations that express the propagation of sound wave are solved without acoustic source in the far field. Figure 9 shows the far field pressure fluctuations predicted by the Lighthill's and Powell's acoustic analogy. The DNS result is also presented for comparison. The far-field pressure fluctuation predicted by the Lighthill's acoustic analogy excellently agrees with the result of DNS. However, the pressure fluctuation predicted by the Powell's acoustic analogy is significantly smaller than that obtained by DNS. This is because the entropy term that dominates the acoustic source is not included in the Powell's acoustic analogy as shown in Eq. (10). Therefore, the Powell's acoustic analogy is not applicable for turbulent flames.

To evaluate the contributions of each acoustic source term on the predicted sound wave, the far field pressure fluctuations predicted by the Reynolds stress term and the entropy term are shown separately in Fig. 10. The predicted pressure fluctuation by the Reynolds stress term is significantly small compared with that by the entropy term. These results coincide with the observation that the entropy term is significantly larger than the Reynolds stress term shown in Fig. 4. However, in the later stage of the transition to turbulence ($45 < t < 70$), the Reynolds term should be included to predict the sound more precisely.

3. Noise Reduction by Passive Control of Turbulence

As shown in the previous section, the dominant sound sources in the turbulent combustion field are the entropy term due to the heat release rate and turbulent dissipation rate, and Reynolds stress term due to the coherent fine scale eddies. In this project, the final objective is the establishment of the active control techniques of the combustors with suppressing combustion noise and combustion-driven oscillations. Before applying active control, it is important to reduce combustion noise by passive controls of turbulence. Therefore, in this study, the passive controls are applied for the coaxial dump combustor in National Maritime Research Institute as a preliminary step. The coaxial dump combustor used in this study is shown in Fig. 11. Detailed descriptions of the combustor can be found in Kishi *et al.* 2001. The passive controls are conducted by setting a mesh before the combustion chamber because turbulent intensity is quite high in the combustion chamber for the original setup. It was considered that the high turbulence level lead to large fluctuation of heat release rate and large energy dissipation rate, which result in the sound source as shown in the previous section.

Measurements of the sound level are conducted for hydrogen-air premixed flames with $0.18 < \phi < 0.42$.

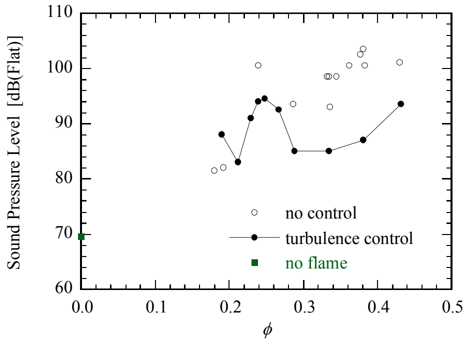

Fig. 13 Sound pressure levels of the dominant modes for no control and turbulence control (hydrogen-air flame).

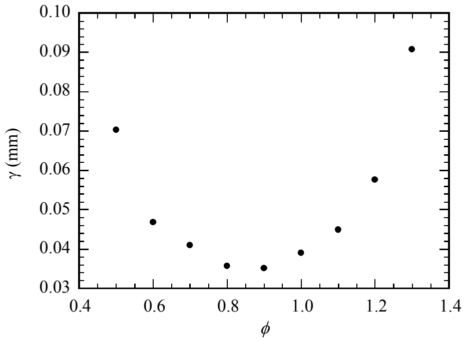

Fig. 14 Distance between peaks of the heat release rate and CH mole fraction in laminar CH_4-air premixed flames (PREMIX, GRI mech. 2.11).

The turbulent intensity on the centerline decreases to about 5% of the mean velocity from 13% of the original setup by setting the mesh. Figure 12 shows spectrums of the combustion-induced noise for no control case and for turbulence control case for ϕ=0.4. For ϕ=0.4, the natural frequency of 106Hz resonates with the combustion-induced sound and dominates the sound field for no control case. The sound levels decrease about 25dB at the peak frequency (f=106Hz) by the turbulence control. However, the several peaks remain even for the case of turbulence control. The peaks in Fig. 12 correspond to the natural frequencies of the combustor. In Fig. 13, the sound level of the dominant resonance mode is shown for different equivalence ratio. For ϕ>0.28, distinct decreases of the dominant mode can be observed. However, effects of the turbulence control are not clear for ϕ<0.28. The abrupt increase of the dominant mode at about ϕ=0.24 should be controlled actively.

To develop the active control scheme of combustor, estimations of the heat release rate in the combustor is required because suppressions of the combustion-induced noise and combustion-driven oscillation of combustor are essential for stable lean combustion. In this study, measurements of spatial and temporal fluctuations of the heat release rate will be conducted by planar laser-induced fluorescence by changing the fuel to methane from hydrogen.

4. Estimations of the Heat Release Rate in Turbulent Flames by PLIF

4.1 Heat release rate and CH concentration

Relationships between the heat release rate and CH concentration are investigated by numerical simulations of methane-air premixed flames. Figure 14 shows the distance between peaks of the heat release rate and CH mole fraction in one-dimensional laminar methane-air premixed flames. Numerical simulations are conducted by using PREMIX in CHEMKIN. For a kinetic mechanism, GRI mechanism ver. 2.11 is used. The mixture of methane and air is set equal to be 0.1MPa and 298.15K. The distance of the peaks becomes the minimum value of 35μm for ϕ=0.9. For ϕ<0.9 and ϕ>0.9, the distance tends to increase, while it is 70μm for ϕ=0.5 and 91μm for ϕ=1.3. These results suggest that CH concentration is a good indicator of the heat release rate.

In turbulent flames, heat release rate fluctuates along the flame front since the local flame structure significantly affected by turbulence in the unburned gas (Tanahashi *et al.* 1999). In this study, relation between the heat release rate and CH concentration is investigated by two-dimensional DNS of a methane-air turbulent premixed flame with a detailed kinetic mechanism. A methane-air reaction mechanism which includes 279 elementary reactions (GRI mechanism ver. 2.11) is employed. The GRI mechanism includes 49 chemical species, so 48 sets of conservation equations for mass fraction are solved directly with mass, momentum and energy conservation equations, and the equation of the state. The viscosity, the thermal conductivity and the diffusion coefficients are calculated by CHEMKIN FORTRAN packages (Kee *et al.* 1986, 1989), where original programs are modified to be fully vectorized and parallelized. Details of the numerical method are shown in Tanahashi *et al.* (1999). Inflow boundary conditions for the chemical species are set equal to methane-air mixture with equivalent ratio of ϕ=1.0 at 0.1MPa and 298.15K. Inflow turbulence is set to be u'/S_L=30 and l/δ_L=4.80.

The distributions of the heat release rate and CH mole fraction in the methane-air turbulent premixed flame obtained by DNS are shown in Figs. 15 (a) and (b). Even for the premixed flame in high intensity turbulence, the distribution of the heat release rate coincides with that of CH mole fraction. In Fig. 15(c), the flame front (Green lines), which is defined by the local maximum temperature gradient, is plotted with local maximum lines of the heat release rate (Blue lines) and the CH mole fraction (Red lines). Behind the preheat zone, the local maximum line of the heat release rate exists, and the local maximum line of CH is located just after that of the heat release rate. The two local maximum lines are nearly parallel and

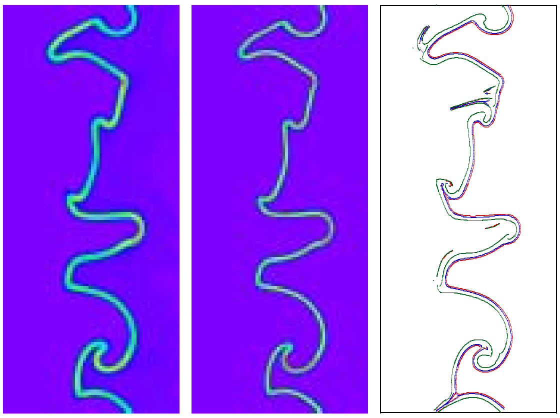

Fig. 15 Distributions of the heat release rate (a), CH mole fraction (b) and relation between peaks of the heat release rate and CH mole fraction(c) in a turbulent CH_4-air premixed flame (DNS, GRI mech. 2.11). In (c), Blue: heat release rate, Red: X_{CH} and Green: flame fronts

Fig. 16 The laser system for CH-OH planar laser-induced fluorescence measurements in Tokyo Institute of Technology.

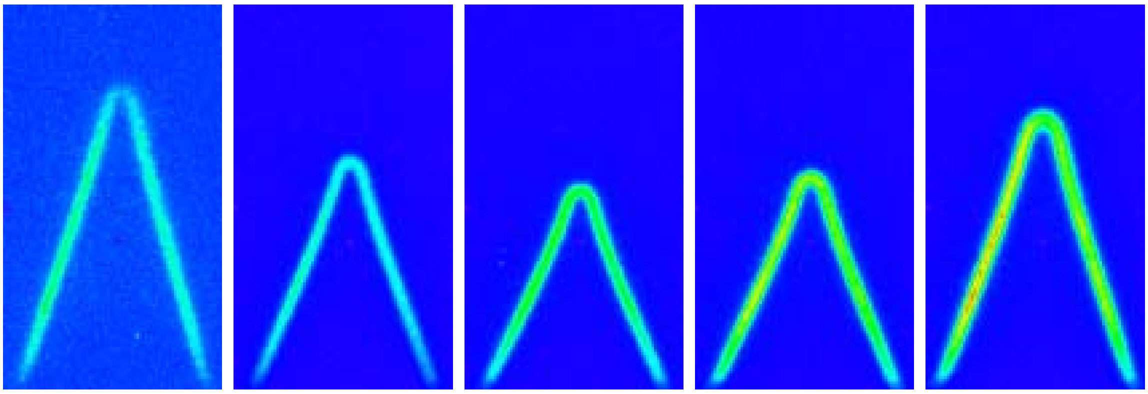

ϕ=0.8 ϕ=0.9 ϕ=1.0 ϕ=1.1 ϕ=1.2

Fig. 17 CH fluorescence images for CH_4-air premixed flames with different equivalence ratio in a slot burner.

distance between them is sustained to be nearly that of the corresponding laminar flame. These results show that CH concentration is a good indicator of the heat release rate even in the turbulent premixed flames.

4.2 Experimantal method of CH planar laser-induced fluorescence measurements

Figure 16 shows the laser systems for CH/OH PLIF measurements used in this study. For CH PLIF, the $Q_1(7.5)$ transition of the $B^2\Sigma^-$-$X^2\Pi(0,0)$ band at 390.30nm was excited and fluorescence from the A-X(1,1), (0,0) and B-X(0,1) bands between 420 and 440 nm was recorded, which has been proposed by Garland & Crosley (1985) and Carter *et al.* (1998). Many groups have conducted successful CH PLIF measurements using this transition (Watson *et al.* (2000), Han & Mungal (2000)). Two laser source systems were used for excitation. The one system consists of an Nd-YAG laser (Sectra-Physics, Quanta Ray PRO-101, 532nm, 350mJ/pulse) and a dye laser (Sireah Precisionscan), and generates laser pulses with about 12.5mJ/pulse. The other system consists of a XeCl excimer laser (Lambda Phisik, LPX 110i, 308nm, 200mJ/pulse) and a dye laser (Lambda Phisik, Scanmate 2), and generates laser pulses with about 23-25 mJ/pulse. In the present study, we show the results from a XeCl excimer-pumped dye laser system with BiBuQ dye in p-Dioxane solvent, of which pulse width is 10-20ns. The collection optics was located perpendicular to the laser sheet. An intensified CCD camera (Andor Technology, DH734-25U-03) with 105mm F4.5 UV lens was used for the imaging. In order to block the flame radiation, 3mm thick interference filter (KV-418 Scott) was used. To optimize signal-to-noise ratio, all measurements were conducted with an image intensifier gate time of 30ns; this value was determined by preliminary experiments with a different gate time. The experiments were performed in a slot burner and a flat burner (McKenna). Laser sheets for the slot burner and flat burner were approximately 8mm wide - 200μm thick and 4mm wide - 200 μm thick, respectively.

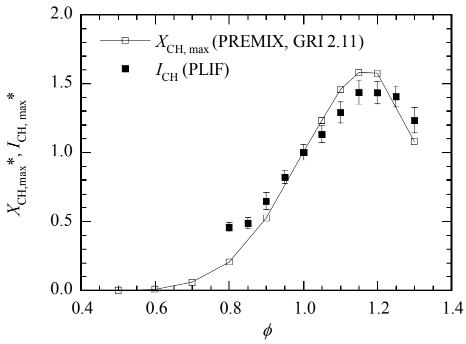

Fig. 18 CH mole fraction obtained by numerical simulations of one dimensional laminar flame with GRI 2.11 and CH fluorescence intensity by PLIF.

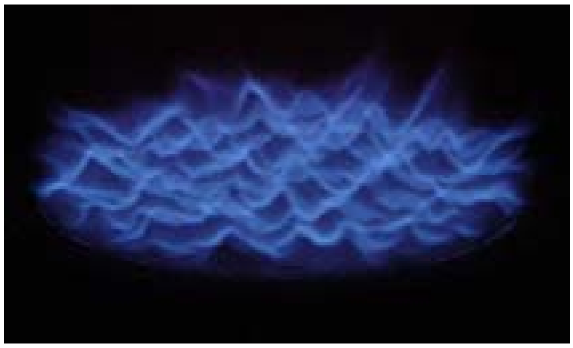

Fig. 19 Direct photograph of the unsteady cellular flame in a flat burner (ϕ=0.65).

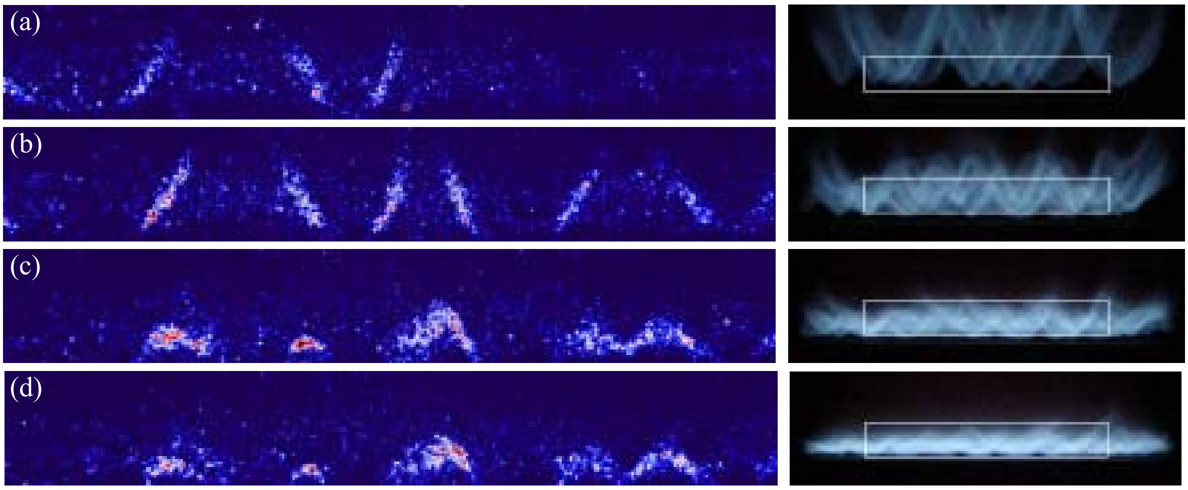

Fig. 20 CH fluorescence images (left side) and direct photographs (right side) of the unsteady cellular flames on a flat burner. (a): ϕ=0.60, (b): ϕ=0.65, (c): ϕ=0.70 and (d): ϕ=0.75. White boxes in direct photographs represent the displayed regions in CH fluorescence images.

4.3 Fundamental aspects of CH PLIF measurements

Figure 17 shows the CH PLIF images for different equivalence ratio in the slot burner. In each case, 100 images are averaged. For all range of equivalence ratio measured in this study, CH fluorescence can be captured clearly and intensity of CH fluorescence depends on the equivalence ratio. It should be noted that ϕ=0.8 is nearly the lower limit of the flame stabilization in the slot burner used in this study. In Fig. 18, the maximum CH mole fraction obtained by numerical simulations of the laminar flame with GRI mechanism ver. 2.11 and the maximum intensity of CH fluorescence obtained by PLIF measurements are compared. Mole fractions and fluorescence intensities are normalized by the values of ϕ=1.0. The trend of the fluorescence intensity agrees with that of CH mole fraction computed with GRI mechanism, which implies that CH PLIF intensity can represents difference of CH mole fraction due to the equivalence ratio.

With the increase of the flow rate, the flame formed on a flat burner becomes unstable for lean conditions and shows unsteady cellular structure as shown in Fig. 19. To estimate distribution of the heat release rate in the turbulent combustion field, it is required for the CH PLIF measurement to capture the spatial fluctuation of CH concentration in unsteady lean flames. Therefore, in this study, CH PLIF measurements are conducted for the unsteady flames in the flat burner for $0.60<\phi<0.75$. Figure 20 shows the CH fluorescence images and corresponding direct photographs. White boxes in direct photographs represent the displayed regions in CH fluorescence images. Here, the height of the CH fluorescence image is 6mm, and there are no laser sheets in 2mm from the upper size. The direct photographs show that flame becomes unstable and locally detaches from the burner surface with the decrease of the equivalence ratio. The CH fluorescence images well represent this phenomenon. Even for the lean condition, in which CH mole fraction significantly decreases compared with that in ϕ=1.0, CH fluorescence can be measured. These results imply that CH PLIF measurements can be applicable for the estimation of the heat release fluctuations in the turbulent combustion field.

5. Summary

In this study, DNS are extended for investigations of the sound generation in the turbulent combustion. From DNS of a compressible and chemically reacting turbulent mixing layer, the mechanism of the sound generation in the turbulent flames is clarified. The effects of heat release on the mechanism of sound generation are investigated in fully developed turbulent state. The contributions of sound source terms are investigated from DNS results. The acoustic source is dominated by the entropy term. The distributions of the Reynolds stress term and the entropy term are investigated by focusing on the heat release rate and the coherent fine scale eddy in turbulence. The Reynolds stress term shows similar structure with the coherent fine scale eddies. The distribution of the entropy term is mainly dominated by the heat release rate, while it is affected by the energy dissipation rate around the coherent fine scale eddy in the region with low heat release rate. The far field pressure fluctuation was also predicted using acoustic analogies. By comparing the predicted far field sound with DNS result, Lighthill's and Powell's acoustic analogies are evaluated. For turbulent flames, the far field sound seems to be predicted only by considering the entropy term, while the Reynolds term should be included to predict the sound radiated in the process of the transition to turbulence.

Based on the investigation on the sound generation mechanism in turbulent flames, a passive control is applied to a coaxial dump combustor and noise reductions are demonstrated as a preliminary step for developing the active control scheme of the combustor. The sound levels decrease about 25dB at the peak frequency (f=106Hz) by the turbulence control. However, the several peaks remain even for the case of turbulence control. These peaks correspond to the natural frequencies of the combustor. Effects of the turbulence control are not clear in the lean conditions and the abrupt increase of the dominant mode can be observed. It is suggested that this behavior should be controlled actively.

Finally, effectiveness of CH PLIF measurement as for an indicator of the heat release rate is shown by comparing results of CH PLIF experiments and numerical simulations including DNS with a detailed kinetic mechanism. From CH PLIF experiments in the slot burner, it is shown that CH PLIF intensity can represents difference of CH mole fraction due to the equivalence ratio. CH PLIF measurements are conducted for the unsteady flames in the flat burner for $0.60<\phi<0.75$. Even for the lean condition, in which CH mole fraction significantly decreases compared with that in ϕ=1.0, CH fluorescence can be measured. The results in the present study imply that CH PLIF measurements can be applicable for the estimations of the heat release fluctuations in the turbulent combustion field.

References

Allen, M., Howe, R. D. and Hanson, R. K. (1986), Opt Lett. 11:126-128.

Baum, M., Poinsot, T. and Thevenin, D. (1994), J. Comp. Phys. 116: 247-261.

Carter, C. D., Donbar, J. M. and Driscoll, J. F. (1998), Appl. Phys. B, 66: 129-132.

Colonius, T., Lele, S. K. and Moin, P. (1994), J Fluid Mech 260: 271-298

Colonius, T., Lele, S. K. and Moin, P. (1997), J Fluid Mech 330: 375-409

Crigthon, D. G. (1975), Prog. Energy Aerospace Sci. 16: 31-96.

Engquist, B. and Majda, A. (1979), Commun. Pure Applied Math. 23: 313-357.

Garland, N. L. and Crosley, D. R. (1985), Appl. Optics, 24: 4229-4237.

Han, D. and Mungal, M. G. (2000), Proc. Combust. Inst. 28: 261-267.

Harper, J., Johnson, C., Neumeier, Y., Lieuwen, T., and Zinn, B. T. (2001), AIAA Paper-01-0486.

Kee, R. J., Dixon-Lewis, G., Warnatz, J., Coltrin, M. E. and Miller, J. A. (1986), Sandia Report, SAND86-8246.

Kee, R. J., Rupley, F. M. and Miller, J. A. (1989), Sandia Report, SAND89-8009B

Kishi, T., Hiraoka, K., Ikame, M., Harumi, K., Shirota, H. and Oka, H. (2001), Proc. 2nnd Symp. Smart Control of Turbulence: 89-94.

Lee, J. G., Kim K., and Santavicca, D. A. (2000), Proc. Combust. Inst. 28: 739-746.

Li, Y., Tanahashi, M. and Miyauchi, T. (2000), Trans. Jpn. Soc. Mech. Eng. 66B: 2117-2124.

Li, Y., Tanahashi, M. and Miyauchi, T. (2001), JSME Int. J. 44B: 505-512.

Lighthill M J (1952), Proc R Soc Lond A 211: 564-587

Lighthill, J. (1978), Waves in Fluids. Cambridge University Press, 1-5

Lilley, G. M. (1994), Theoret. Comput. Fluid Dynamics, 6: 281-301.

Mansour, M. S., Peters, N. and Chen, Y.-C. (1998), Proc. Combust. Inst. 27: 676-773.

McMurtry, P. A., Riley, J. J. and Metcalfe, R. W. (1989), J. Fluid Mech. 199: 297-332.

Mitchell, B. E, Lele, S. K. and Moin, P. (1995), J Fluid Mech 285: 181-202

Papamoschou, D. and Roshko, A. (1988), J. Fluid Mech. 197: 453-477.

Paschereit, C. O., Gutmark, E., and Weisenstein, W. (1999), Physics Fluids, 11-9: 2667-2678.

Poinsot T J, Lele S K (1992), J. Comp. Phys 101: 104-129

Powell, A. (1964), J Acoust Soc Am 36: 177-195
Tanahashi, M. and Miyauchi, T. (1995), Proc. of the ASME/JSME, Thermal Engineering: 105-110.
Tanahashi, M. Miyauchi, T. & Matsuoka, K. (1997a), Heat and Mass Transfer, Vol. 2, 461-470, Delft University Press.
Tanahashi, M. Miyauchi, T. & Ikeda J. (1997b), Proc. 11th Turbulent Shear Flows 1: 4-12
Tanahashi, M., Saito, T., Shimamura, M. and Miyauchi, T. (1999), Proc. 2nd Asia-Pacific Conference on Combustion: 500-503.
Tanahashi, M., Fujimura, M. and Miyauchi, T. (2000), Proc. Combust. Inst. 28: 529-535.
Tanahashi, M., Iwase, S. and Miyauchi, T. (2001), J. Turbulence 2: 006.
Watson, K. A., Lyons, K. M., Donbar, J. M. and Carter, C. D. (2000), Comb. Flame, 123: 252-265.